HHS Public Access

Author manuscript

Exp Eye Res. Author manuscript; available in PMC 2024 May 01.

Published in final edited form as:

Exp Eye Res. 2023 May ; 230: 109462. doi:10.1016/j.exer.2023.109462.

Sigma 1 Receptor activation improves retinal structure and function in the *Rho*$^{P23H/+}$ mouse model of autosomal dominant retinitis pigmentosa

Shannon R Barwick, Ph.D.[1,2], **Haiyan Xiao**[1,2], **David Wolff**[1], **Jing Wang**[1,2], **Elizabeth Perry**[1], **Brendan Marshall**[1], **Sylvia B. Smith**[1,2,3]

[1]Department of Cellular Biology and Anatomy, Medical College of Georgia, Augusta University, Augusta, GA.

[2]James and Jean Culver Vision Discovery Institute, Augusta University, Augusta, GA.

[3]Department of Ophthalmology, Medical College of Georgia, Augusta University, Augusta, GA

Abstract

Retinitis pigmentosa (RP) is a group of devastating inherited retinal diseases that leads to visual impairment and oftentimes complete blindness. Currently no cure exists for RP thus research into prolonging vision is imperative. Sigma 1 receptor (Sig1R) is a promising small molecule target that has neuroprotective benefits in retinas of rapidly-degenerating mouse models. It is not clear whether Sig1R activation can provide similar neuroprotective benefits in more slowly-progressing RP models. Here, we examined Sig1R-mediated effects in the slowly-progressing *Rho*$^{P23H/+}$ mouse, a model of autosomal dominant RP. We characterized the retinal degeneration of the *Rho*$^{P23H/+}$ mouse over a 10 month period using three *in vivo* methods: Optomotor Response (OMR), Electroretinogram (ERG), and Spectral Domain-Optical Coherence Tomography (SD-OCT). A slow retinal degeneration was observed in both male and female *Rho*$^{P23H/+}$ mice when compared to wild type. The OMR, which reflects visual acuity, showed a gradual decline through 10 months. Interestingly, female mice had more reduction in visual acuity than males. ERG assessment showed a gradual decline in scotopic and photopic responses in *Rho*$^{P23H/+}$ mice. To investigate the neuroprotective benefits of Sig1R activation in the *Rho*$^{P23H/+}$ mouse model, mutant mice were treated with a high-specificity Sig1R ligand (+)-pentazocine ((+)-PTZ) 3x/week at 0.5mg/kg and examined using OMR, ERG, SD-OCT. A significant retention of visual function was observed in males and females at 10 months of age, with treated females retaining ~50% greater visual acuity than non-treated mutant females. ERG revealed significant retention of scotopic and photopic b-wave amplitudes at 6 months in male and female *Rho*$^{P23H/+}$ mice treated with (+)-PTZ. Further, *in vivo* analysis by SD-OCT revealed a significant retention of outer nuclear layer (ONL) thickness in male and female treated *Rho*$^{P23H/+}$ mice. Histological studies showed significant retention of IS/OS length (~50%), ONL thickness, and number of

Please send correspondence to: Shannon R. Barwick, Ph.D., Department of Cellular Biology and Anatomy, Medical College of Georgia at Augusta University, 1120 15th Street, CB1811, Augusta, GA 30912-2000, 706-721-3078 (phone), sbarwick@augusta.edu.

rows of photoreceptor cell nuclei at 6 months in (+)-PTZ-treated mutant mice. Interestingly, electron microscopy revealed preservation of OS discs in (+)-PTZ treated mutant mice compared to non-treated. Taken collectively, the *in vivo* and *in vitro* data provide the first evidence that targeting Sig1R can rescue visual function and structure in the $Rho^{P23H/+}$ mouse. These results are promising and provide a framework for future studies to investigate Sig1R as a potential therapeutic target in retinal degenerative disease.

Keywords

photoreceptor cells; visual acuity; retinal degeneration; rhodopsin P23H; (+)-pentazocine

Introduction

Retinitis pigmentosa (RP), a group of devastating inherited retinal degenerative diseases, leads to death of rod photoreceptor cells (rod/cone dystrophy) or the death of cone photoreceptor cells (cone/rod dystrophy) (Guafagni et al, 2016). RP can be inherited as autosomal dominant (adRP), autosomal recessive (arRP), or X-linked. The majority of RP cases are autosomal recessive; adRP cases comprise the second largest number of cases with most mutations occurring in the RHO gene and are non-syndromic RP (Mendes et al, 2005). RP typically leads to the loss of rod photoreceptor cells initially with subsequent loss of cones (Hamel, 2006). It presents most often in early adulthood and patients complain of night blindness and decreased peripheral vision. The progression of RP is typically slow but due to the heterogeneous nature of the disease it is difficult to predict (van Soest et al, 1999). Currently, no cure exists for RP and therapies focus on stem cell therapy (Carr et al, 2013; Zakrzewski et al 2019), gene therapy (Latella et al, 2016; Vandenberghe et al, 2011: Yu et al. 2017) and retinal implants (Hallum and Dakin 2021). While these are promising approaches, therapeutic targets are a propitious option that can also benefit a wide range of RP patients with varying disease origins.

Sigma 1 receptor (Sig1R) is a unique protein with robust neuroprotective retinal properties (Smith et al, 2018). It is a small (~27kD) transmembrane protein with no known mammalian homologs. Sig1R is a pluripotent modulator of cell survival (Su et al, 2016) and has been classified as a novel target for treatment of neurodegenerative diseases (Nguyen et al, 2015). It is abundantly expressed throughout the eye including all retinal cell types, notably photoreceptors (Ola et al, 2001; Wang et al. 2002).

The first report addressing whether Sig1R modulates photoreceptor cell survival *in vivo* was from Hara's group. They administered SA4503, a Sig1R ligand, intravitreally in wild type mice 1h prior to inducing photoreceptor cell death with intense light exposure. They reported improved dark-adapted ERGs and decreased photoreceptor cell loss in SA4503-treated v. non-treated mice (Shimazawa et al, 2015). Sig1R-mediated retinal protection has been investigated in genetic models of photoreceptor cell degeneration. Our lab utilized the $Pde6b^{rd10/J}$ (*rd10*) mouse model to test activation of Sig1R (Wang et al, 2016). The *rd10* mouse has a mutation in the beta subunit of the cGMP-phosphodiesterase gene (Chang et al, 2002; Chang et al, 2007) and develops a rapid photoreceptor cell degeneration.

Upon treatment with a high affinity Sig1R ligand (+)-pentazocine ((+)-PTZ), mice showed improved photopic ERGs and histological assessment revealed cone preservation (Wang et al, 2016). To confirm that cone photoreceptor cell protection was directly related to Sig1R activation, our lab generated *rd10* mice lacking Sig1R (*rd10/Sig1R*$^{-/-}$). These mice were treated with/without (+)-PTZ and showed no improvement in photopic ERG and no cone preservation suggesting Sig1R is required for (+)-PTZ-mediated cone rescue (Wang et al, 2016). The Guo lab also investigated lack of Sig1R in *rd10* mice (reared in dim light to reduce rapid photoreceptor cell loss) and found that *rd10/Sig1R*$^{-/-}$ mice had a retinal phenotype that was worse than *rd10/Sig1R*$^{+/+}$ mice (Yang et al, 2017).

The *rd10* mouse provided compelling evidence that activation of Sig1R is potentially therapeutic though the degenerative process is quite rapid. The current study explored the role of Sig1R-mediated retinal neuroprotection in a model with a more slowly progressing disease that more faithfully recapitulates RP in humans, the *Rho*-P23H mouse model. The P23H mutation of rhodopsin accounts for ~10% of all cases of adRP (Chen et al, 2014).

A number of laboratories have attempted to create an adRP model with the P23H mutation of rhodopsin (Barwick et al, in press), and the one established by the Palczewski laboratory authentically recapitulates the human disease. A cohort of 19 human adRP patients with the RHO-P23H mutation were evaluated in conjunction with the knock-in *Rho*-P23H mouse model that was generated. The mouse demonstrates a slowly progressing loss of ERG function over many months, similar to patients carrying the *Rho*$^{P23H/+}$ mutation, and a slow progressive retinal degeneration in which gradual shortening and disorganization of outer segments precedes rod photoreceptor cell death. A notable feature of the *Rho*$^{P23H/+}$ mouse model is that its degeneration pattern shows regional retinal degenerative differences such that the ventral (inferior) retina degenerates more rapidly than the dorsal (superior) retina, which is similar to the inferior-superior differences observed in human RP patients (Sakami et al. 2011). In aggregate, the aforementioned similarities of the humanized mouse model created in the Palczewski laboratory to human adRP patients (Dias et al, 2017) make this model a particularly attractive tool for investigating mechanisms of disease and interventional strategies.

The present work investigated Sig1R activation in this model. Earlier reports of the *Rho*$^{P23H/+}$ mouse reported ERG responses in a small number of mice, however no other functional tests were performed. Here, we conducted comprehensive functional and morphological assessments of the retinal degeneration over a 10 month period and evaluated consequences of Sig1R activation in the *Rho*$^{P23H/+}$ model.

Materials and methods

Animal Breeding

Rho$^{P23H/P23H}$ and wild type (C57BL/6J) mice were purchased from Jackson Laboratories (strain number 017628, 000664; Bar Harbor, ME). *Rho*$^{P23H/P23H}$ male mice were crossed with wild type females to produce *Rho*$^{P23H/+}$ offspring. Maintenance and treatment of animals adhered to institutional guidelines for humane treatment of animals and to the ARVO statement for Use of Animals in Ophthalmic and Vision Research.

395 mice were used in this study. Mice were evaluated utilizing functional assessments every month from 1–10 months of age. Due to the gradual decline in visual acuity observed over the 10 month time period, further functional and histological analysis was performed at 2, 4, 6, 8, and 10 months (n~286). Mice usage for each experiment is outlines in Supplementary Table 1.

Administration of (+)-Pentazocine

(+)-PTZ (6-methano-3-benzazocin-8-ol, Sigma Aldrich, St. Louis, MO), dissolved in DMSO and diluted in 0.01M PBS, was administered intraperitoneally at a dosage of 0.5mg/kg three times per week beginning on postnatal day 14 (P14) for the duration of the mouse's life.

Visual Acuity

Visual acuity of wild type, $Rho^{P23H/+}$, and $Rho^{P23H/+}$ + (+)-PTZ-treated mice was measured as spatial thresholds for opto-motor tracking of sine-wave gratings using a virtual optokinetic system (OptoMotry, CerebralMechanics, Medicine Hat, Alberta, Canada) (Prusky et al, 2004). Mice were analyzed as described in earlier studies (Navneet et al, 2019; Xiao et al, 2020). Briefly, the unrestrained mouse was placed on a small platform at the epicenter of the chamber. The chamber (comprised of four computer monitors) produced vertical sine-wave gratings moving at 12°/s or gray of the same mean luminance creating a virtual cylinder. Grating rotation elicited reflexive optomotor tracking, which was scored via live video using the two-alternative forced choice procedure. Data were recorded as the highest SF that yields optomotor tracking responses on 70% of the trials, determined by a staircase procedure.

Electrophysiology (ERG)

Electrophysiological studies were performed to evaluate photoreceptor cell (and other retinal neuronal) responses *in vivo* in mice (ages 2, 4, 6, 8, and 10 months). Retinal cell function was investigated using the Diagnosys Celeris ERG system (Lowell, MA) as described previously (Wang et al, 2020). Briefly, mice were dark-adapted overnight and anesthetized with 80 mg/kg ketamine and 10 mg/kg xylazine. 2.5% Phenylephrine Hydrochloride Ophthalmic Solution and 2% Tropicamide Ophthalmic Solution were used to dilate the pupils. Probes, containing both electrode and light source, were placed on the cornea with 0.3% hypromellose (GenTeal®Tears). Dark adapted scotopic scans using a series of light flashes with increasing intensities (e.g. 0.001, 0.005, 0.01, 0.1, 0.5, 1 cd s/m^2) were performed. Following scotopic analysis, photopic scans were performed using a series of light flashes with increasing intensities (e.g. 3, 10, 25, 50, 100, 150 cd s/m^2).

Spectral Domain-Optical Coherence Tomography (SD-OCT)

SD-OCT was performed to evaluate retinal structure *in vivo* in mice at ages 2, 4, 6, 8, and 10 months. Mice were anesthetized as described for ERG. Retinal architecture was assessed *in vivo* using a Bioptigen Spectral Domain Ophthalmic Imaging System (SDOIS; Bioptigen Envisu Leica, R2200, Buffalo Grove, IL), which includes averaged single B-scan and volume intensity scans with images centered on the optic nerve head as described previously (Wang et al, 2020). Post-imaging analysis included manual assessment of retinal

layers using InVivoVue™ Diver 2.4 software (Bioptigen). Five measurements each were taken at (1) the level of dorsal retina, (2) level of the optic nerve, and (3) level of the ventral retina using the caliper function.

Orientation and processing of tissue for light microscopy

A Stemi 2000-C (Zeiss) stereo microscope was utilized to visualize the eye of the euthanized mouse. A small burn at the dorsal limbus was made using a GEMINITM Cautery Pen System to permit orientation of the eye. Eyes were removed and placed immediately in optimal cutting temperature compound (OCT) (Elkhart, IN). They were flash frozen without fixation and 10μm thick cryosections were obtained.

Morphology

Retinal cryosections, stained with hematoxylin and eosin, were used to perform morphometric analyses. Two images were captured from the dorsal and ventral retina per eye of using a Zeiss Axio Imager D2 microscope (Carl Zeiss, Göttingen, Germany) equipped with a high-resolution camera. Two measurements per image were taken of the total retinal thickness, ONL thickness, and IS/OS length. Additionally, the number of rows of photoreceptor cell nuclei were counted. Measurements were performed using the distance function of the Zeiss Zen 2.3 Pro software.

Electron Microscopy Preparation, Embedding and Visualization

Eyes that had been oriented as described were fixed in 4% paraformaldehyde, 2% glutaraldehyde in 0.1 M sodium cacodylate (NaCac) buffer, pH 7.4, postfixed in 2% osmium tetroxide in NaCac, stained in block with 2% uranyl acetate, dehydrated with a graded ethanol series and embedded in Epon-Araldite resin. The block was trimmed to permit proper orientation of the eye during imaging. Thin sections were cut with a diamond knife on a Leica EM UC7 ultramicrotome (Leica Microsystems, Inc, Bannockburn, IL), collected on copper grids and stained with uranyl acetate and lead citrate. Tissue was observed in a JEM 1400 flash transmission electron microscope (JEOL USA Inc., Peabody, MA) at 110 kV and imaged with a CMOS CCD camera & One View Digital Camera Controller (Gatan Inc., Pleasanton, CA). Images were taken within the IS/OS region of dorsal retinas. Images focused on the OS were used to qualitatively assess the organization and density of OS.

Statistical Analysis

Data were collected and statistical analysis was performed using two-way ANOVA with multiple comparisons. Due to sex differences that were observed in this study, data were separated into male and female groups and multicomparison factors used were age and treatment. Tukey’s post-hoc test was utilized. Data were considered significant if the P-value was less than 0.05.

Results

Male and female Rho$^{P23H/+}$ mice retain visual acuity with (+)-PTZ treatment.

Visual acuity was investigated using the OptoMotry system in wild type, *Rho*$^{P23H/+}$, *Rho*$^{P23H/+}$ + (+)-PTZ mice. Wild type mice evaluated in this study had visual acuity averaging ~0.4 c/d over the 10 month testing period (Fig. 1A and C), which is consistent with expected values. Visual acuity in male *Rho*$^{P23H/+}$ mice was similar to wild type through 2 months with a slight decline between 3 and 6 months averaging ~0.35 c/d. A highly significant reduction in visual acuity was observed in male *Rho*$^{P23H/+}$ averaging ~0.25 c/d at 10 months when compared to wild type (Fig. 1A). Visual acuity was similar in (+)-PTZ-treated and non-treated male *Rho*$^{P23H/+}$ mice at 1–3 months. By 4 months, acuity was significantly better in treated mice (Fig. 1B). At 10 months visual acuity in male mutant mice was ~0.24 c/d, whereas (+)-PTZ-treated mutant mice demonstrated visual acuity that was ~0.33 c/d ($p=0.0004$).

Visual acuity in female *Rho*$^{P23H/+}$ mice was similar to wild type through 4 months and was slightly lower than observed in mutant males (Fig. 1C). Visual acuity declined steadily from 5–8 months. The decline progressed rapidly such that by 10 months, the visual acuity in females averaged less than 0.1 c/d while age-matched males averaged ~0.25 c/d.

Visual acuity was significantly retained in female *Rho*$^{P23H/+}$ mice treated with (+)-PTZ at 4 months (~0.4 c/d). Visual acuity declined in female *Rho*$^{P23H/+}$ mice to less than 0.1 c/d at 10 months, whereas (+)-PTZ treated mutant mice showed significant preservation of acuity greater than 0.2 c/d at 10 months ($p<0.0001$, Fig. 1D). It should be noted that to our knowledge this is the first report of differences between male and female in the *Rho*$^{P23H/+}$ mouse model, hence data are presented for the two sexes separately throughout this report. Due to the gradual decline in visual acuity over the 10 months studied, the studies that followed were performed at ages 2, 4, 6, 8, and 10 months.

Male and female Rho$^{P23H/+}$ mice retain visual function with (+)-PTZ treatment.

Photoreceptor cell function was analyzed by ERG in wild type, *Rho*$^{P23H/+}$, and *Rho*$^{P23H/+}$ + (+)-PTZ mice. Scotopic and photopic analyses were performed to investigate rod and cone function in male and female mice. Representative tracings for scotopic and photopic data for male mice are shown in supplementary figures 1 and 2 while quantitative data are shown in figures 2 and 3. Wild type male mice had robust scotopic responses over the 10 months studied with a b-wave amplitude ranging from ~400–500μV at the highest flash intensities. Male *Rho*$^{P23H/+}$ mice showed a gradual decline in scotopic b-wave amplitudes over the 10 months tested (Fig. 2A–E). By 10 months there was a marked decrease in scotopic responses in *Rho*$^{P23H/+}$ males compared to age-matched wild type male mice.

At 6 months, non-treated mutant male mice showed a decline in the scotopic b-wave amplitudes averaging ~140μV, yet (+)-PTZ treated *Rho*$^{P23H/+}$ mice showed robust amplitudes most noticeable at the highest flash energy (~200μV, 1 cd.s/m^2, Fig. 2H). A similar trend was observed in 8-month mice (~90μV v. ~150μV for non-treated v. treated, Fig. 2I). At 10 months, differences between treated and non-treated groups were no longer detectible. There were no changes in implicit time (Sup. Fig. 7). Scotopic a-wave was

analyzed in male *Rho*$^{P23H/+}$ non-treated and treated mice. No significant changes were observed throughout the 10 month testing period.

Wild type male mice had robust photopic responses over the 10 months studied with a b-wave amplitude ranging from ~80–100μV at the highest flash intensities (Fig. 3A–E). Photopic b-wave amplitudes in male *Rho*$^{P23H/+}$ mice were significantly reduced at all ages compared to wild type. Regarding PTZ-treated male *Rho*$^{P23H/+}$ mice, no differences were observed compared to non-treated through 6 months (Fig 3F–H). At 8 months *Rho*$^{P23H/+}$ male mice showed a decline in b-wave amplitudes (~30μV) whereas (+)-PTZ-treated male mice averaged ~55μV (150 cd.s/m^2, Fig. 3I). At 10 months differences between treated and non-treated groups were no longer detected

ERG was performed in female mice and representative tracings for scotopic and photopic responses in female mice are shown in supplementary figures 3 and 4 while quantitative data are shown in figures 4 and 5. Wild type female mice had robust scotopic responses over the 10 months studied. No significant differences were observed in scotopic results between male and female wild type mice (Sup. Fig.8). Scotopic b-wave amplitudes in *Rho*$^{P23H/+}$ female mice gradually declined over the 10 months. Interestingly, scotopic responses declined precipitously between 4 and 6 months such that at 6 months responses ranged from ~30–80μV (Fig. 4C). At 8 and 10 months scotopic responses were barely detectible (1 cd.s/m^2, Fig. 4D–E). Scotopic b-wave amplitudes in female *Rho*$^{P23H/+}$ mice were significantly reduced at all ages when compared to wild type.

Scotopic responses in females at 2 and 4 months were comparable in *Rho*$^{P23H/+}$ mice regardless of (+)-PTZ treatment (Fig. 4F–G). By 6 months, non-treated mutant females showed a decline in the b-wave amplitudes (~80μV), whereas (+)-PTZ treated *Rho*$^{P23H/+}$ mice showed robust amplitudes especially noticeable at the highest flash energy (~150μV, 1 cd.s/m^2, Fig 4H). Similarly, at 8 months *Rho*$^{P23H/+}$ females had b-wave amplitudes of ~40μV at the highest flash intensities whereas (+)-PTZ-treated mutant mice were significantly better (~60–80μV at 1 cd.s/m^2, Fig. 4I). At 10 months, differences between treated and non-treated groups were no longer detectible. There were no changes in implicit times (Sup. Fig 7). Scotopic a-waves were analyzed in female treated and non-treated *Rho*$^{P23H/+}$ mice and revealed little change over the 10 months. A significant retention of scotopic a-wave amplitudes was observed only at 6 months in (+)-PTZ treated mice (~35μV, 1 cd.s/m^2, Sup. Fig. 6C).

Photopic b-wave amplitudes in wild type female mice had robust responses over 10 months ranging from 90–100μV at the highest flash intensities (Fig. 5 A–E). Photopic responses in female *Rho*$^{P23H/+}$ mice showed a gradual decline in b-wave amplitudes over the 10 months tested. Collectively, these results suggest that ERG responses gradually decline over the 10 month testing period in both male and female *Rho*$^{P23H/+}$ mice.

At 2 months, non-treated mutants had an average b-wave amplitude of ~50μV, while (+)-PTZ-treated *Rho*$^{P23H/+}$ mice had more robust amplitudes particularly at the highest flash energy (~100μV, 150 cd.s/m^2, Fig. 5F). By 6 months, non-treated female mutants had b-wave amplitudes averaging ~40μV, while (+)-PTZ-treated mutants were significantly higher

averaging ~60μV at the highest flash energy (150 cd.s/m^2, Fig 5H). When female mutant mice were analyzed at 10 months, there were no significant differences between treated and non-treated mice. Taken collectively, the ERG analyses showed that (+)-PTZ treatment significantly improved scotopic and photopic responses in male and female *Rho*$^{P23H/+}$ mice, with most improvement seen between 6 and 8 months.

Male and female Rho$^{P23H/+}$ mice retain ONL thickness with (+)-PTZ treatment through 10 months of age.

Initial studies to investigate whether the inner or outer retina of *Rho*$^{P23H/+}$ mice using SD-OCT revealed no changes within the inner retina, but a decrease in the outer retinal thickness. We speculated this is likely occurring within the ONL or IS/OS region or both. The SD-OCT has limited resolution for IS/OS length, which limits accurate measurement of this region. To overcome this limitation, we focused our measurements on the ONL layer.

Sakami et al. (2011) noted differences in dorsal vs. ventral retinas in P23H mice. Therefore, OCT measurements of the ONL thickness were made in the dorsal, optic nerve head and ventral retina regions in males and females, respectively. Representative images of SD-OCT performed in male wild type, *Rho*$^{P23H/+}$, and *Rho*$^{P23H/+}$ + (+)-PTZ mice are shown in supplementary figures 9A and 10A and quantified in supplementary figure 9A and figure 6. Wild type males showed an ONL thickness ~60μm that was maintained throughout the 10 month testing period (Sup. Fig 9A). Dorsal ONL thickness in *Rho*$^{P23H/+}$ male mice decreased to approximately half that of wild type mice in all retinal regions as early as 2 months (Fig. 6A) and gradually declined through 10 months. ONL thickness in (+)-PTZ-treated male *Rho*$^{P23H/+}$ mice was significantly thicker (~20μm). In treated and non-treated *Rho*$^{P23H/+}$mice the ONL thickness declines in a gradual manner from thickest in the dorsal retina to thinnest in the ventral retina.

Representative images of SD-OCT performed in female wild type, *Rho*$^{P23H/+}$, and *Rho*$^{P23H/+}$ + (+)-PTZ mice are shown in supplementary figures 9B and 10B and quantified in supplementary figure 9B and figure 7. Wild type females had an ONL thickness ~60μm that was maintained throughout the 10 months tested (Sup. Fig 9B). Female *Rho*$^{P23H/+}$ mice have a marked decline in ONL thickness between 2 and 4 months from ~20μm to ~10μm (Fig. 7A and 7B) and gradually declined through 10 months. Female *Rho*$^{P23H/+}$ ONL thickness declined at a faster rate than males. Data from SD-OCT analyses of mutant and treated female *Rho*$^{P23H/+}$ mice revealed (+)-PTZ-treated *Rho*$^{P23H/+}$ females had significantly thicker ONL than non-treated, age-matched mutants in dorsal, optic nerve, and ventral retinal regions (Fig. 7). The ONL in (+)-PTZ treated *Rho*$^{P23H/+}$ females was significantly thicker through 8 months. Thus, for both male and female mutants, activation of Sig1R has a beneficial effect in preserving cells within the ONL.

Male and female Rho$^{P23H/+}$ mice retain photoreceptor cell nuclei number and IS/OS length with (+)-PTZ treatment through 6 months of age.

Morphometric analyses were performed on H&E-stained retinal sections from wild type, *Rho*$^{P23H/+}$, and *Rho*$^{P23H/+}$ + (+)-PTZ-treated mice. Total retinal thickness, ONL thickness, IS/OS length, and number of rows of photoreceptor cell nuclei were measured over 10

months in male and female mice. The dorsal and ventral regions were analyzed separately. Representative images are shown in supplementary figure 11 (2, 4, 8, 10 months) and figure 8 (6 months). Quantification of thickness of the total retina, ONL, IS/OS length, and the number of rows of photoreceptor cell nuclei are presented in supplementary figures 12 (2, 4, 8, 10 months) and figure 8 (6 months).

The retinas of wild type male mice typically measure ~200–250μm in thickness. The ONL is ~40–60μm and IS/OS are ~30–40μm (Sup. Fig. 12 and Fig. 8). Wild type mice typically have 10–12 rows of photoreceptor cell nuclei. In contrast, *Rho*$^{P23H/+}$ male mice demonstrate a decline in rows from 2 to 10 months. The ventral retina of mutants declined more rapidly than dorsal at least through the first 6 months. In PTZ-treated mice, measurements of the ONL, IS/OS and number of rows of photoreceptor cells were consistently greater than non-treated through 6 months. For example, at 4 months there were 5 rows of nuclei in the dorsal region and only 3 in the ventral region of non-treated mutants, whereas there were 7 and 5 rows in the dorsal and ventral regions, respectively, in age-matched (+)-PTZ-treated mutants (Sup. Fig. 12).

Another important observation from the data in figure 8 is the significantly longer IS/OS in the dorsal retina of (+)-PTZ-treated male mutant mice (~25μm) versus non-treated (~12μm) at 6 months (Fig. 8D). These morphometric results suggest significant preservation of the outer retina when Sig1R is activated in male *Rho*$^{P23H/+}$ mice through ~6 months of age.

Data from retinal morphological analyses in female mutant mice administered (+)-PTZ versus non-treated are presented in supplementary figures 13–14 and figure 8. Wild type female mice and had well organized retinas over the 10 month study with the total retinal thickness averaging ~200–225μm. Wild type female mice had an ONL thickness of ~40–50μm and IS/OS length of ~40μm. There were 10–12 rows of photoreceptor cell nuclei (Sup. Fig. 14 and Fig. 8)

Non-treated *Rho*$^{P23H/+}$ female mice showed few differences when compared to (+)-PTZ-treated age-matched mutants at 2 and 4 months. At 6 months, IS/OS were significantly longer in PTZ-treated *Rho*$^{P23H/+}$ female mice in the dorsal retina (~20μm) compared to non-treated mutants (~11μm). At that same age there were 6 rows of photoreceptor cell nuclei in (+)-PTZ-treated female mice versus ~3.5 in non-treated mutants. By 8 months, there were no differences in retinal thickness, ONL thickness, IS/OS length, or number of rows of photoreceptor cell nuclei between the treated and non-treated groups.

Male and female Rho$^{P23H/+}$ mice retain OS organization with (+)-PTZ treatment through 6 months of age.

Sakami et al. previously reported disorganization of the *Rho*$^{P23H/+}$ mouse OS discs (Sakami et al, 2011). Utilizing EM in P63 *Rho*$^{P23H/+}$ mice, instances of perpendicularly-oriented discs, elongated discs, and vesicles within the OS disc area were observed. To investigate whether Sig1R activation mitigates this disorganization, retinas were evaluated by EM in wild type 4 month male and female *Rho*$^{P23H/+}$ and *Rho*$^{P23H/+}$ (+)-PTZ-treated mice. The assessment was made at 4 months because it was the first age at which benefit of Sig1R activation was observed in the OMR response and in the OCT measurements of ONL

thickness. Wild type retinal OS typically contain stacks of discs (flattened membranes, flattened membranous lamellae) that are radially oriented (Patt and Patt, 1969). The spacing between discs is generally uniform (Gartner and Hiatt, 2001). As expected, wild type retinas had radially-oriented discs stacked upon each other; spacing was uniform (the inner segments are also well-organized (Sup. Fig 15).

EM images of the inner and outer segments are shown for male $Rho^{P23H/+}$ mice (Fig. 9). Selected areas are highlighted (red insets) and shown as increasing magnifications in adjacent panels. EM analysis showed inner segments similar to those of (+)-PTZ treated male $Rho^{P23H/+}$ mice (Fig. 9A, 9D) whereas outer segments were shorter and thinner than treated mutants. In many areas, discs were disorganized in the non-treated group (arrows Fig. 9C). $Rho^{P23H/+}$ OS are not tightly stacked compared to wild type and each disc does not span the area within the plasma membrane that enshrouds the disc. Instead, the discs and are often broken off into vesicles. Indeed, in some places vacuolated areas have replaced the disorganized discs. In (+)-PTZ treated male $Rho^{P23H/+}$ mice, outer segments were considerably more abundant than in non-treated mice. They were frequently organized as tightly-packed stacks of flattened discs. While vesicles were occasionally observed, they were in non-treated mutants. This level of outer segment integrity was observed throughout the PTZ-treated retinas.

EM images of the inner and outer segments are shown for female $Rho^{P23H/+}$ mice in figure 10. EM analysis showed inner segments that were similar to those of (+)-PTZ treated $Rho^{P23H/+}$ mice (Figs. 10A, 10D) though outer segments were fewer. The female non-treated $Rho^{P23H/+}$ mice had outer segment disorganization, with numerous vesicles replacing well-organized discs in many regions (Fig. 10C). Regions of disorganization were markedly increased in $Rho^{P23H/+}$ female mutants compared to males. In (+)-PTZ treated females, vesicles were occasionally observed, but were less abundant when compared to non-treated mutants and few areas of disorganization were observed. Discs were often organized as tightly packed stacks of flattened discs (Fig 10F). Note closely packed outer segments are observed in female (+)-PTZ treated $Rho^{P23H/+}$ retina (Fig. 10D), which can be appreciated in figures 10E and 10F. This level of outer segment integrity was observed throughout the retina.

Discussion

Sig1R is a promising therapeutic target implicated in neuroprotection in neurodegenerative diseases (Maurice et al, 1996; Maurice et al, 1998; Wang et al, 2003; Francardo et al, 2014). Our lab and others previously investigated whether Sig1R affords neuroprotection for rapidly-progressing degenerative eye diseases. Here, a more slowly-progressing model of RP, the $Rho^{P23H/+}$ mouse model, was used to test how generalizable Sig1R activation is in protecting rod and cone degeneration. The first aim of the current work was to comprehensively characterize degeneration in this slowly-progressing, clinically-relevant RP model and the second aim was to test the retinal neuroprotective effects of Sig1R activation in terms of function as well as structure.

The comprehensive assessment of retinal function of the *Rho*$^{P23H/+}$ mouse compared to wild type mice spanned a 10-month period and utilized three assessments: OMR, ERG and SD-OCT. Analysis of visual acuity measured as OMR in *Rho*$^{P23H/+}$ mice revealed a steady decline when compared to wild type mice. Interestingly, the analysis of visual acuity, revealed sex differences in this mutant that have not been reported previously. Female *Rho*$^{P23H/+}$ mice degenerated more rapidly than males, but in both cases the acuity loss was gradual. The more pronounced degeneration observed in female *Rho*$^{P23H/+}$ mice has not been reported in human *RHO*$^{P23H/+}$ patients. The slow progressive loss of visual acuity observed in *Rho*$^{P23H/+}$ mice more faithfully mimics the typical presentation in human adRP patients than other P23H models (Dias et al, 2017), underscoring its usefulness for therapeutic intervention studies. While this is the first report of assessment of visual acuity in *Rho*$^{P23H/+}$ mice, it is important to note that OMR has been investigated in the *Rho*$^{P23H/P23H}$ mice previously by Charish and colleagues (Charish et al, 2020). Their findings revealed visual acuity in *Rho*$^{P23H/P23H}$ was less than age-matched *rd10* mice.

The second aim of this work was to investigate consequences of Sig1R activation on retinal function and structure in *Rho*$^{P23H/+}$ model. Significant retention of scotopic and photopic ERG data was observed between 6 and 8 months in male and female treated mutant mice. This suggests that not only cone photoreceptor cells were preserved in this model when Sig1R was activated, but also some rod function was preserved as demonstrated by mixed cone and rod responses at high scotopic flash intensities and scotopic a-wave data. This was not observed in *rd10* mice treated with (+)-PTZ, in which only cones were preserved (Wang et al, 2016; Wang et al, 2017). The *rd10* mutation is homozygous, thus the cGMP-PDE mutation is present in every rod photoreceptor cell and the degeneration occurs within a few weeks' time. In contrast, the *Rho*$^{P23H/+}$ mutation affects half of the rod photoreceptor cells (*Rho*$^{P23H/+}$ versus *Rho*$^{P23H/P23H}$). The resulting heterozygous degeneration is slower and spans several months. Our findings are important since loss of rod function and subsequently cone function is a feature of human adRP. Nevertheless, photoreceptor cell function was clearly enhanced with Sig1R activation.

SD-OCT analysis provided important insights into benefits of Sig1R activation in *Rho*$^{P23H/+}$ mice. In both (+)-PTZ-treated males and females there was a significant increase in the ONL thickness through 10 months. Notably, improvements were observed in ventral retina as well as dorsal. Thus, Sig1R activation offered pan-retinal protection in this mutant. Although robust protection was observed via SD-OCT, histological analysis of the ONL was less robust. It is impressive to observe benefit at 6 months, an age significantly beyond the benefit observed in *rd10* mice. To observe a near doubling of IS/OS length in 6 month males is particularly noteworthy as this is the cellular site of rhodopsin synthesis (inner segment) and sequestration until phototransduction (outer segment). This may suggest there is still a gradual loss of photoreceptor cell number, but the cells that are preserved maintain their IS/OS length. Shortening of IS/OS has been observed as a characteristic precursor to photoreceptor cell loss (Sakami et al, 2011).

Our light microscopy studies were complemented by EM analyses. Earlier work had described disorganization of OS discs in the *Rho*$^{P23H/+}$ mutant (Sakami et al, 2011). The EM analysis performed for this project focused on this retinal region as well. The analysis

of (+)-PTZ-treated *Rho*$^{P23H/+}$ mice revealed preservation of disc integrity in males and females. To our knowledge, this is the first report that Sig1R activation can preserve disc structure in the retina. In the *Rho*$^{P23H/+}$ mouse, the mutant rhodopsin is misfolded and does not incorporate properly into outer segment discs. The proper integration of rhodopsin is integral to OS disc morphology. It is possible that Sig1R activation improves protein folding in this model, but this remains to be tested. The entire outer segment disc renewal process could be evaluated in this mutant mouse to determine effects of Sig1R activation on this critical process.

This work provides evidence that Sig1R activation can delay photoreceptor cell degeneration in the *Rho*$^{P23H/+}$ mouse and complements earlier studies demonstrating retinal neuroprotection in other models (Shimazawa et al, 2015; Wang et al, 2016). The findings support Sig1R as a promising target for retinal disease. An important contribution of the present study was the comprehensive assessment of retinal function as well as histologic evaluation over an extended time period. adRP is a progressive disease and typically spans many decades. Hence, it is important to determine the extent of therapeutic benefits. Recent studies have reported therapies for the *Rho*$^{P23H/+}$ strain (used in this work, i.e. generated by the Palczewski laboratory), but none have described results past ~4 months of age (Ortega et al, 2022, Lee et al, 2021, Qiu et al, 2019).

There are limitations of the current study, which set the stage for future work. First, this project focused on characterization of retinal phenotype and did not investigate mechanisms of photoreceptor cell degeneration. Some studies of the *Rho*$^{P23H/+}$ mice have investigated ER stress and autophagy as mechanisms of the degeneration (Sakami et al, 2011, Yao et al, 2018). These mechanisms could be investigated in future studies of Sig1R activation in this model. In studies of the more severe *rd10* mouse model of autosomal recessive RP, Sig1R was shown to modulate the key antioxidant protein NRF2 (Wang et al, 2017; Wang et al, 2019; Wang et al, 2020; Xiao et al, 2020), It is possible that such a mechanism is relevant to Sig1R-mediated neuroprotection in the *Rho*$^{P23H/+}$ mouse as well. Now that the time course of the degeneration and the effects of Sig1R are established, studies could be conducted at select ages.

A second limitation of the study is that only one Sig1R agonist was investigated, which was (+)-PTZ. It is logical to initiate a study analyzing Sig1R activation using this compound because of its high specificity and affinity for Sig1R (Su 1982). It is the prototypical Sig1R agonist. It would be worthwhile to assess newer Sig1R ligands. For example, there are exciting data from the Levin lab showing the Sig1R ligand, pridopidine, was effective in protecting retinal ganglion cells in two rodent models of glaucoma (Geva et al, 2021). Additionally, evaluating effects of Sig1R activation on outer segment renewal, shedding and phagocytosis in *Rho*$^{P23H/+}$ mice could yield important insights into effects of this unique molecule on photoreceptor cell biology.

Supplementary Material

Refer to Web version on PubMed Central for supplementary material.

Acknowledgments

This work was supported by the National Institutes of Health (National Eye Institute, R01 EY012830 and P30 EY031631), and the James and Jean Culver Vision Discovery Institute of Augusta University. We acknowledge the EM/Histology Core (Department of Cellular Biology and Anatomy, Medical College of Georgia at Augusta University) for the excellent instrumentation and technical assistance in tissue processing and EM imaging acquisition.

References

Carr AJ, Smart MJ, Ramsden CM, Powner MB, da Cruz L, Coffey PJ., 2013. Development of human embryonic stem cell therapies for age-related macular degeneration. Trends Neurosci. 36(7):385–95. doi: 10.1016/j.tins.2013.03.006. [PubMed: 23601133]

Chang B, Hawes NL, Hurd RE, Davisson MT, Nusinowitz S, Heckenlively JR., 2002. Retinal degeneration mutants in the mouse. Vision Res. 42(4):517–25. doi: 10.1016/s0042-6989(01)00146-8. [PubMed: 11853768]

Chang B, Hawes NL, Pardue MT, German AM, Hurd RE, Davisson MT, Nusinowitz S, Rengarajan K, Boyd AP, Sidney SS, Phillips MJ, Stewart RE, Chaudhury R, Nickerson JM, Heckenlively JR, Boatright JH., 2007. Two mouse retinal degenerations caused by missense mutations in the beta-subunit of rod cGMP phosphodiesterase gene. Vision Res. 47(5):624–33. doi: 10.1016/j.visres.2006.11.020. [PubMed: 17267005]

Charish J, Shabanzadeh AP, Chen D, Mehlen P, Sethuramanujam S, Harada H, Bonilha VL, Awatramani G, Bremner R, Monnier PP., 2020. Neogenin neutralization prevents photoreceptor loss in inherited retinal degeneration. J Clin Invest.130(4):2054–2068. doi: 10.1172/JCI125898. [PubMed: 32175920]

Chen Y, Jastrzebska B, Cao P, Zhang J, Wang B, Sun W, Yuan Y, Feng Z, Palczewski K., 2014. Inherent instability of the retinitis pigmentosa P23H mutant opsin. J Biol Chem. 28;289(13):9288–303. doi: 10.1074/jbc.M114.551713.

Dias MF, Joo K, Kemp JA, Fialho SL, da Silva Cunha A Jr, Woo SJ, Kwon YJ., 2018. Molecular genetics and emerging therapies for retinitis pigmentosa: Basic research and clinical perspectives. Prog Retin Eye Res. 63:107–131. doi: 10.1016/j.preteyeres.2017.10.004. [PubMed: 29097191]

Francardo V, Bez F, Wieloch T, Nissbrandt H, Ruscher K, Cenci MA., 2014. Pharmacological stimulation of sigma-1 receptors has neurorestorative effects in experimental parkinsonism. Brain. 137(Pt 7):1998–2014. doi: 10.1093/brain/awu107. [PubMed: 24755275]

Gargini C, Terzibasi E, Mazzoni F, Strettoi E., 2007. Retinal organization in the retinal degeneration 10 (rd10) mutant mouse: a morphological and ERG study. J Comp Neurol. 500(2):222–38. doi: 10.1002/cne.21144. [PubMed: 17111372]

Gartner LP, Hiatt JL., 2001. Color Textbook of Histology (2nd ed.). W.B Saunders Company.

Geva M, Gershoni-Emek N, Naia L, Ly P, Mota S, Rego AC, Hayden MR, Levin LA., 2021. Neuroprotection of retinal ganglion cells by the sigma-1 receptor agonist pridopidine in models of experimental glaucoma. Sci Rep. 11(1):21975. doi: 10.1038/s41598-021-01077-w. [PubMed: 34753986]

Hamel C, 2006. Retinitis pigmentosa. Orphanet J Rare Dis. 1:40. [PubMed: 17032466]

Latella MC, Di Salvo MT, Cocchiarella F, Benati D, Grisendi G, Comitato A, Marigo V, Recchia A., 2016. In vivo Editing of the Human Mutant Rhodopsin Gene by Electroporation of Plasmid-based CRISPR/Cas9 in the Mouse Retina. Mol Ther Nucleic Acids. 5(11): e389. doi: 10.1038/mtna.2016.92. [PubMed: 27874856]

Lee EJ, Chan P, Chea L, Kim K, Kaufman RJ, Lin JH., 2021. ATF6 is required for efficient rhodopsin clearance and retinal homeostasis in the P23H rho retinitis pigmentosa mouse model. Sci Rep. 11(1):16356. doi: 10.1038/s41598-021-95895-7. [PubMed: 34381136]

Maurice T, Roman FJ, Su TP, Privat A. Beneficial effects of sigma agonists on the age-related learning impairment in the senescence-accelerated mouse (SAM). Brain Res. 1996 Sep 16;733(2):219–30. doi: 10.1016/0006-8993(96)00565-3. [PubMed: 8891305]

Maurice T, Su TP, Privat A., 1998. Sigma1 (sigma 1) receptor agonists and neurosteroids attenuate B25–35-amyloid peptide-induced amnesia in mice through a common mechanism. Neuroscience. 83(2):413–28. doi: 10.1016/s0306-4522(97)00405-3. [PubMed: 9460750]

Mendes HF, van der Spuy J, Chapple JP, Cheetham ME., 2005. Mechanisms of cell death in rhodopsin retinitis pigmentosa: implications for therapy. Trends Mol Med. 11(4):177–85. doi: 10.1016/j.molmed.2005.02.007. [PubMed: 15823756]

Navneet S, Zhao J, Wang J, Mysona B, Barwick S, Ammal Kaidery N, Saul A, Kaddour-Djebbar I, Bollag WB, Thomas B, Bollinger KE, Smith SB., 2019. Hyperhomocysteinemia-induced death of retinal ganglion cells: The role of Müller glial cells and NRF2. Redox Biol. 24:101199. doi: 10.1016/j.redox.2019.101199. [PubMed: 31026769]

Nguyen L, Lucke-Wold BP, Mookerjee SA, Cavendish JZ, Robson MJ, Scandinaro AL, Matsumoto RR., 2015. Role of sigma-1 receptors in neurodegenerative diseases. J Pharmacol Sci 127, 17–29. doi: 10.1016/j.jphs.2014.12.005. [PubMed: 25704014]

Ola MS, Moore P, El-Sherbeny A, Roon P, Agarwal N, Sarthy VP, Casellas P, Ganapathy V, Smith SB., 2001. Expression pattern of sigma receptor 1 mRNA and protein in mammalian retina. Brain Res Mol Brain Res. 95(1–2):86–95. doi: 10.1016/s0169-328x(01)00249-2. [PubMed: 11687279]

Olsson JE, Gordon JW, Pawlyk BS, Roof D, Hayes A, Molday RS, Mukai S, Cowley GS, Berson EL, Dryja TP., 1992. Transgenic mice with a rhodopsin mutation (Pro23His): a mouse model of autosomal dominant retinitis pigmentosa. Neuron. 9(5):815–30. doi: 10.1016/0896-6273(92)90236-7. [PubMed: 1418997]

Ortega JT, Parmar T, Carmena-Bargueño M, Pérez-Sánchez H, Jastrzebska B., 2022. Flavonoids improve the stability and function of P23H rhodopsin slowing down the progression of retinitis pigmentosa in mice. 100(4):1063–1083. J Neurosci Res. doi: 10.1002/jnr.25021. [PubMed: 35165923]

Patt DI, Patt GR., 1969. Comparative Vertebrate Histology. Harper and Row Publishing.

Price BA, Sandoval IM, Chan F, Simons DL, Wu SM, Wensel TG, Wilson JH., 2011. Mislocalization and degradation of human P23H-rhodopsin-GFP in a knockin mouse model of retinitis pigmentosa. Investig. ophthalmol. vis. sci. 52(13):9728–36. doi: 10.1167/iovs.11-8654. [PubMed: 22110080]

Prusky GT, Alam NM, Beekman S, Douglas RM, 2004. Rapid quantification of adult and developing mouse spatial vision using a virtual optomotor system. Invest. Ophthalmol. Vis. 45(12):4611–6. doi: 10.1167/iovs.04-0541.

Qiu Y, Yao J, Jia L, Thompson DA, Zacks DN., 2019. Shifting the balance of autophagy and proteasome activation reduces proteotoxic cell death: a novel therapeutic approach for restoring photoreceptor homeostasis. Cell death dis. 10(8):1–4. doi: 10.1038/s41419-019-1780-1.

RetNet. The Information Network. Available online at https://sph.uth.edu/retnet/.

Sakami S, Maeda T, Bereta G, Okano K, Golczak M, Sumaroka A, Roman AJ, Cideciyan AV, Jacobson SG, Palczewski K., 2011. Probing mechanisms of photoreceptor degeneration in a new mouse model of the common form of autosomal dominant retinitis pigmentosa due to P23H opsin mutations. J Biol Chem. 286(12). doi: 10.1074/jbc.M110.209759.

Saul A, Still A., 2016. Multifocal Electroretinography in the presence of temporal and spatial correlations and eye movements. Vision (Basel). 1(1):3. doi: 10.3390/vision1010003. [PubMed: 31740628]

Shimazawa M, Sugitani S, Inoue Y, Tsuruma K, Hara H., 2015. Effect of a sigma-1 receptor agonist, cutamesine dihydrochloride (SA4503), on photoreceptor cell death against light-induced damage. Exp Eye Res. 132:64–72. doi: 10.1016/j.exer.2015.01.017. [PubMed: 25616094]

Smith SB, Wang J, Cui X, Mysona BA, Zhao J, Bollinger KE., 2018. Sigma 1 receptor: A novel therapeutic target in retinal disease. Prog Retin Eye Res. 67:130–149. doi: 10.1016/j.preteyeres.2018.07.003. [PubMed: 30075336]

Su TP., 1982. Evidence for sigma opioid receptor: binding of [3H] SKF-10047 to etorphine-inaccessible sites in guinea-pig brain. J Pharmacol Exp Ther 223:284–290. [PubMed: 6290634]

Su TP, Su TC, Nakamura Y, Tsai SY., 2016. The Sigma-1 receptor as a pluripotent modulator in living systems. Trends Pharmacol Sci 37(4):262–278 doi: 10.1016/j.tips.2016.01.003. [PubMed: 26869505]

van Soest S, Westerveld A, de Jong PT, Bleeker-Wagemakers EM, Bergen AA., 1999. Retinitis pigmentosa: defined from a molecular point of view. Surv Ophthalmol. 43(4):321–34. doi: 10.1016/s0039-6257(98)00046-0. [PubMed: 10025514]

Vandenberghe LH, Bell P, Maguire AM, Cearley CN, Xiao R, Calcedo R, Wang L, Castle MJ, Maguire AC, Grant R, Wolfe JH, Wilson JM, Bennett J., 2011. Dosage thresholds for AAV2 and AAV8 photoreceptor gene therapy in monkey. Sci Transl Med. 3(88):88ra54. doi: 10.1126/scitranslmed.3002103.

Wang HH, Chien JW, Chou YC, Liao JF, Chen CF., 2003. Anti-amnesic effect of dimemorfan in mice. Br J Pharmacol. 138(5):941–9. doi: 10.1038/sj.bjp.0705117. [PubMed: 12642396]

Wang J, Saul A, Cui X, Roon P, Smith SB., 2017. Absence of Sigma 1 Receptor Accelerates Photoreceptor Cell Death in a Murine Model of Retinitis Pigmentosa. Invest Ophthalmol Vis Sci. 58(11):4545–4558. doi: 10.1167/iovs.17-21947. [PubMed: 28877319]

Wang J, Saul A, Roon P, Smith SB., 2016. Activation of the molecular chaperone, sigma 1 receptor, preserves cone function in a murine model of inherited retinal degeneration. Proc Natl Acad Sci U S A. 113(26):E3764–72. doi: 10.1073/pnas.1521749113. [PubMed: 27298364]

Wang J, Xiao H, Barwick SR, Smith SB., 2020. Comparison of Sigma 1 Receptor Ligands SA4503 and PRE084 to (+)-Pentazocine in the rd10 Mouse Model of RP. Invest Ophthalmol Vis Sci. 61(13):3. doi: 10.1167/iovs.61.13.3.

Wang J, Zhao J, Cui X, Mysona BA, Navneet S, Saul A, Ahuja M, Lambert N, Gazaryan IG, Thomas B, Bollinger KE, Smith SB., 2019. The molecular chaperone sigma 1 receptor mediates rescue of retinal cone photoreceptor cells via modulation of NRF2. Free Radic Biol Med. 134:604–616. doi: 10.1016/j.freeradbiomed.2019.02.001. [PubMed: 30743048]

Wang WF, Ishiwata K, Kiyosawa M, Kawamura K, Oda K, Kobayashi T, Matsuno K, Mochizuki M., 2002. Visualization of sigma1 receptors in eyes by ex vivo autoradiography and in vivo positron emission tomography. Exp Eye Res. 75(6):723–30. doi: 10.1006/exer.2002.2048. [PubMed: 12470974]

Xiao H, Wang J, Saul A, Smith SB., 2020. Comparison of Neuroprotective Effects of Monomethylfumarate to the Sigma 1 Receptor Ligand (+)-Pentazocine in a Murine Model of Retinitis Pigmentosa. Invest Ophthalmol Vis Sci. 61(3):5.

Yang H, Fu Y, Liu X, Shahi PK, Mavlyutov TA, Li J, Yao A, Guo SZ, Pattnaik BR, Guo LW., 2017. Role of the sigma-1 receptor chaperone in rod and cone photoreceptor degenerations in a mouse model of retinitis pigmentosa. Mol Neurodegener. 12(1):68. doi: 10.1167/iovs.61.3.5. [PubMed: 28927431]

Yu W, Mookherjee S, Chaitankar V, Hiriyanna S, Kim JW, Brooks M, Ataeijannati Y, Sun X, Dong L, Li T, Swaroop A, Wu Z., 2017. Nrl knockdown by AAV-delivered CRISPR/Cas9 prevents retinal degeneration in mice. Nat Commun. 8:14716. doi: 10.1038/ncomms14716. [PubMed: 28291770]

Zakrzewski W, Dobrzyński M, Szymonowicz M, Rybak Z., 2019. Stem cells: past, present, and future. Stem Cell Res Ther. 10(1):68. doi: 10.1186/s13287-019-1165-5. [PubMed: 30808416]

Highlights

- Retinitis pigmentosa (RP) is a group of inherited retinal degenerative diseases that leads to vision loss and blindness.
- While gene therapy and retinal implants are in progress to slow vision loss due to RP, there is no current cure or effective therapy.
- The *Rho*$^{P23H/+}$ is a clinically relevant model that mimics aspects of human adRP making it useful to study therapeutic targets.
- *Rho*$^{P23H/+}$ mice displayed sexual dimorphisms in which female visual function and structure degenerate more rapidly compared to males.
- Sig1R activation by (+)-PTZ preserved both visual function and retinal architecture in the *Rho*$^{P23H/+}$ mouse model of autosomal dominant RP.

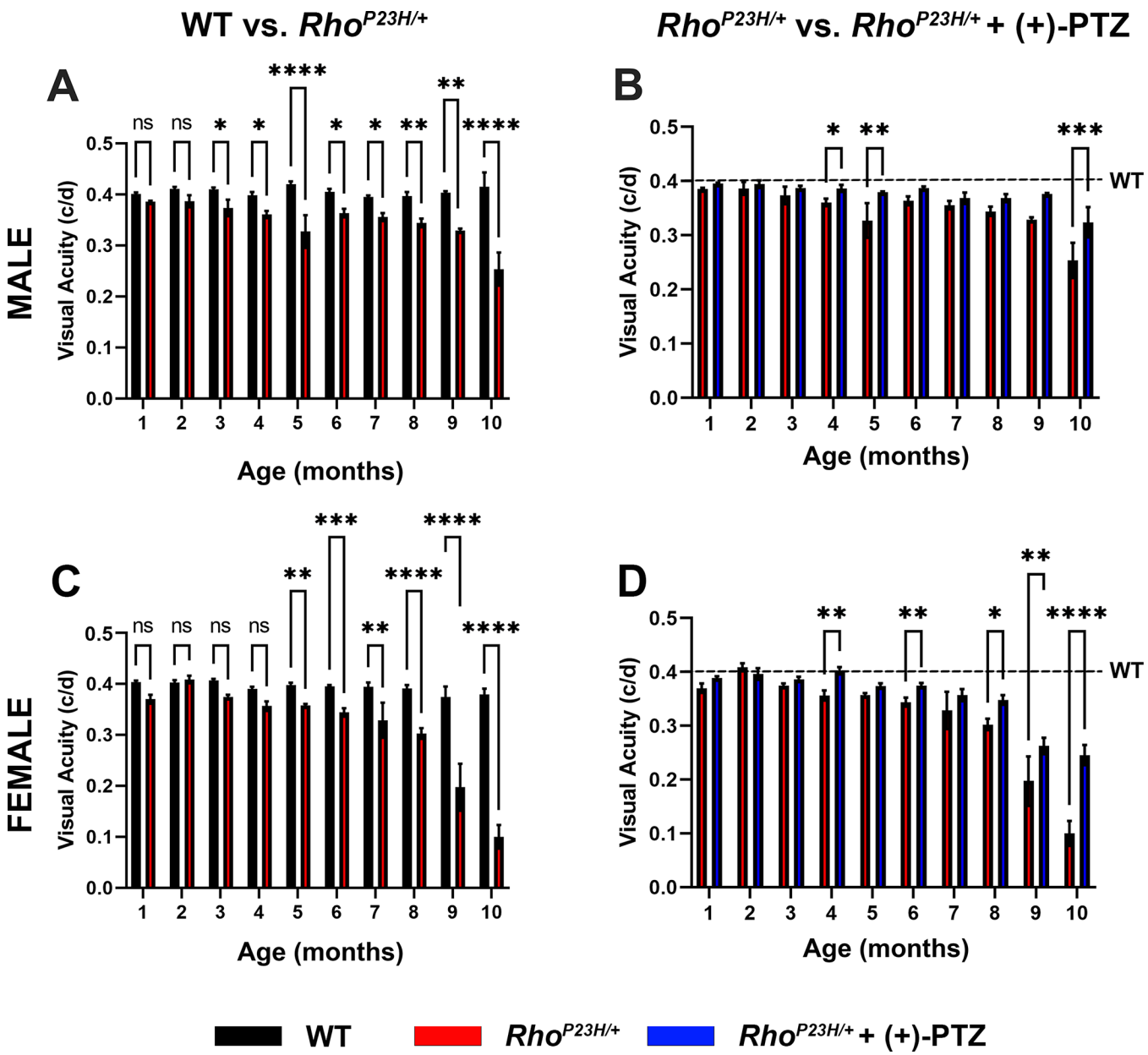

Figure 1: Visual acuity in wild type, *Rho*$^{P23H/+}$ and *Rho*$^{P23H/+}$ + (+)-PTZ mice.

Visual acuity thresholds were measured using the optomotor response and recorded in units of cycles per degree (c/d) in wild type and *Rho*$^{P23H/+}$ mice using the OptoMotry software and apparatus. Data are shown for (A) male *Rho*$^{P23H/+}$ mice, (B) ale *Rho*$^{P23H/+}$ administered (+)-PTZ, (C) female *Rho*$^{P23H/+}$ mice, and (D) female *Rho*$^{P23H/+}$ mice administered (+)-PTZ. In all panels (A-D), wild type values are represented by the black dotted line. Data were considered significant if the P-value was less than 0.05 (*0.05, **0.01, ***0.001, ****0.0001).

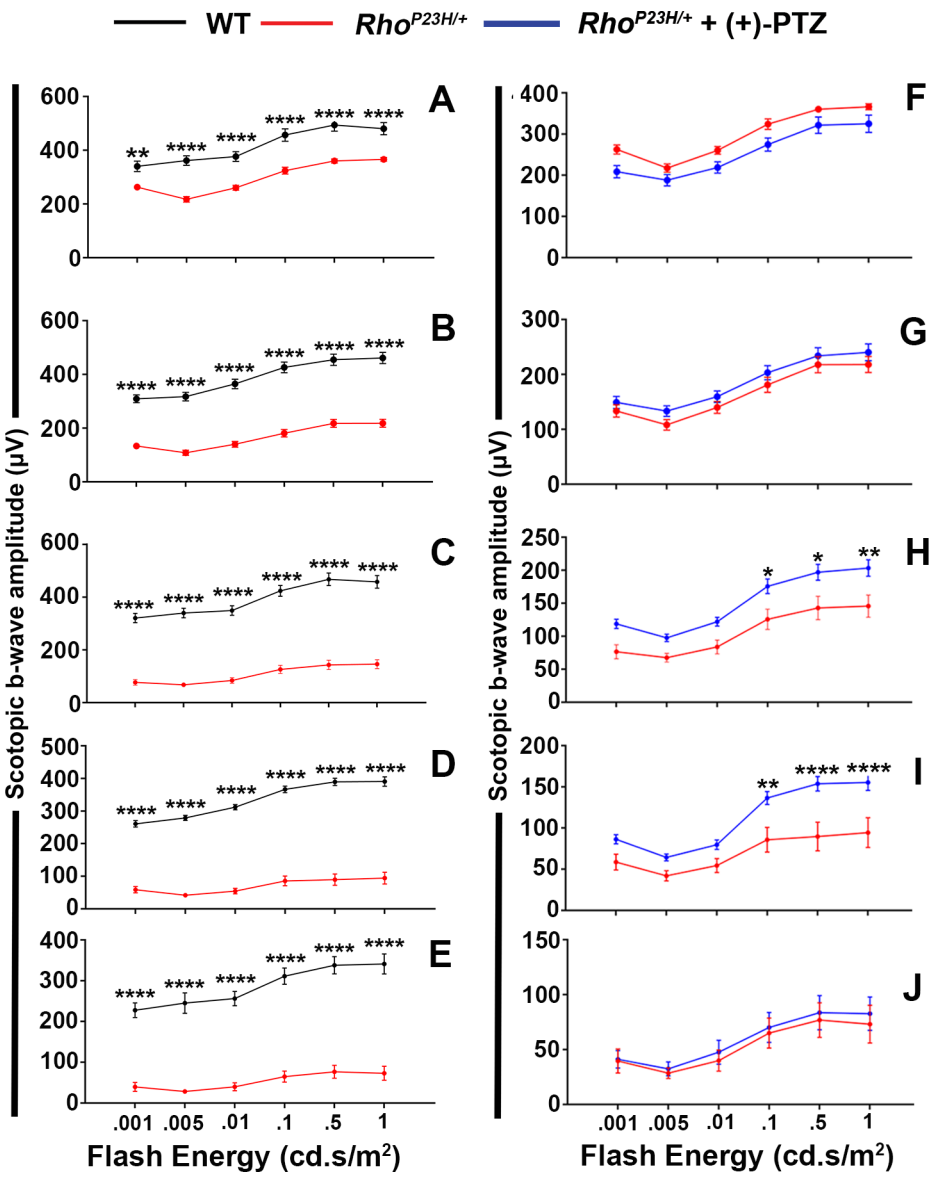

Figure 2: Analysis of scotopic responses in male wild type, *Rho*$^{P23H/+}$ and *Rho*$^{P23H/+}$ + (+)-PTZ mice.

Dark adapted (scotopic) assessment of retinal function in male wild type and *Rho*$^{P23H/+}$ and *Rho*$^{P23H/+}$ + (+)-PTZ mice. Quantitative data from b-wave amplitudes for (A) 2 month (B) 4 month (C) 6 month (D) 8 month (E) 10 month male mice for wild type and *Rho*$^{P23H/+}$ mice plotted at the six light intensities described in the text. Quantitative data from b-wave amplitudes for (F) 2 month (G) 4 month (H) 6 month (I) 8 month (J) 10 month male mice for *Rho*$^{P23H/+}$ and *Rho*$^{P23H/+}$ + (+)-PTZ mice plotted at the six light intensities described in the text. Data were considered significant if the P-value was less than 0.05 (*0.05, **0.01, ***0.001, ****0.0001).

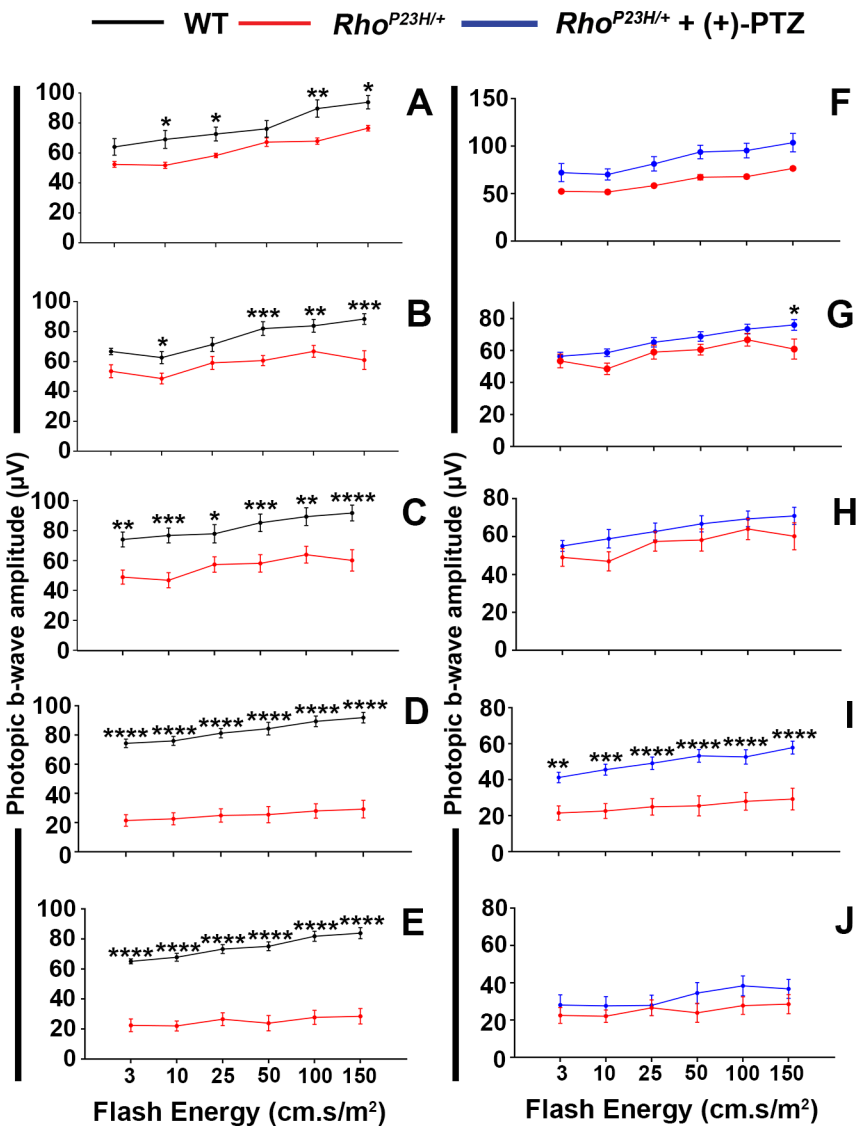

Figure 3: Analysis of photopic responses in male wild type, *Rho*$^{P23H/+}$ and *Rho*$^{P23H/+}$ + (+)-PTZ mice.

Light adapted (photopic) assessment of retinal function in male wild type and *Rho*$^{P23H/+}$ mice and *Rho*$^{P23H/+}$ + (+)-PTZ. Quantitative data from b-wave amplitudes for (A) 2 month (B) 4 month (C) 6 month (D) 8 month (E) 10 month male mice for wild type and *Rho*$^{P23H/+}$ plotted at the six light intensities described in the text. Quantitative data from b-wave amplitudes for (F) 2 month (G) 4 month (H) 6 month (I) 8 month (J) 10 month male mice for *Rho*$^{P23H/+}$ and *Rho*$^{P23H/+}$ + (+)-PTZ plotted at the six light intensities described in the text. Data were considered significant if the P-value was less than 0.05 (*0.05, **0.01, ***0.001, ****0.0001).

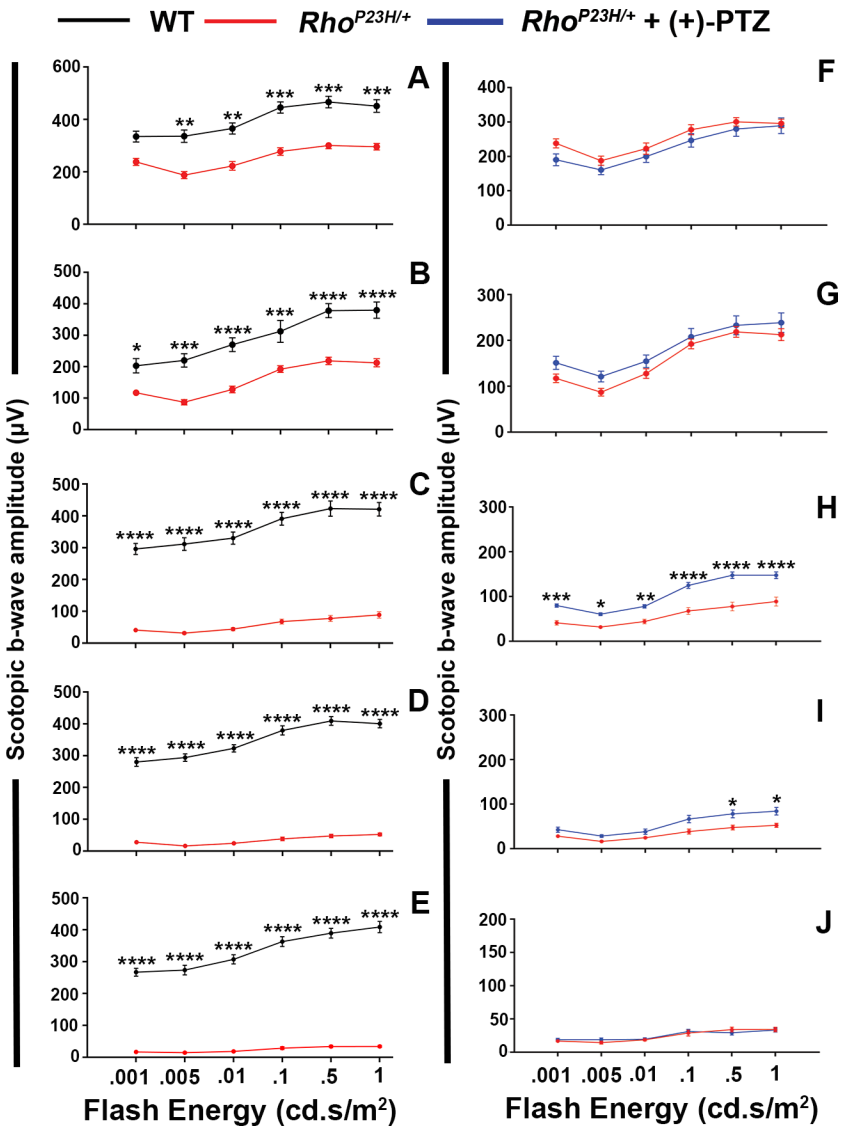

Figure 4: Analysis of scotopic responses in female wild type, *Rho*$^{P23H/+}$ and *Rho*$^{P23H/+}$ + (+)-PTZ mice.

Dark adapted (scotopic) assessment of retinal function in female wild type and *Rho*$^{P23H/+}$ mice and *Rho*$^{P23H/+}$ + (+)-PTZ. Quantitative data from b-wave amplitudes for (A) 2 month (B) 4 month (C) 6 month (D) 8 month (E)10 month female mice for wild type and *Rho*$^{P23H/+}$ plotted at the six light intensities described in the text. Quantitative data from b-wave amplitudes for (F) 2 month (G) 4 month (H) 6 month (I) 8 month (J) 10 month female mice for *Rho*$^{P23H/+}$ and *Rho*$^{P23H/+}$ + (+)-PTZ plotted at the six light intensities described in the text. Data were considered significant if the P-value was less than 0.05 (*0.05, **0.01, ***0.001, ****0.0001).

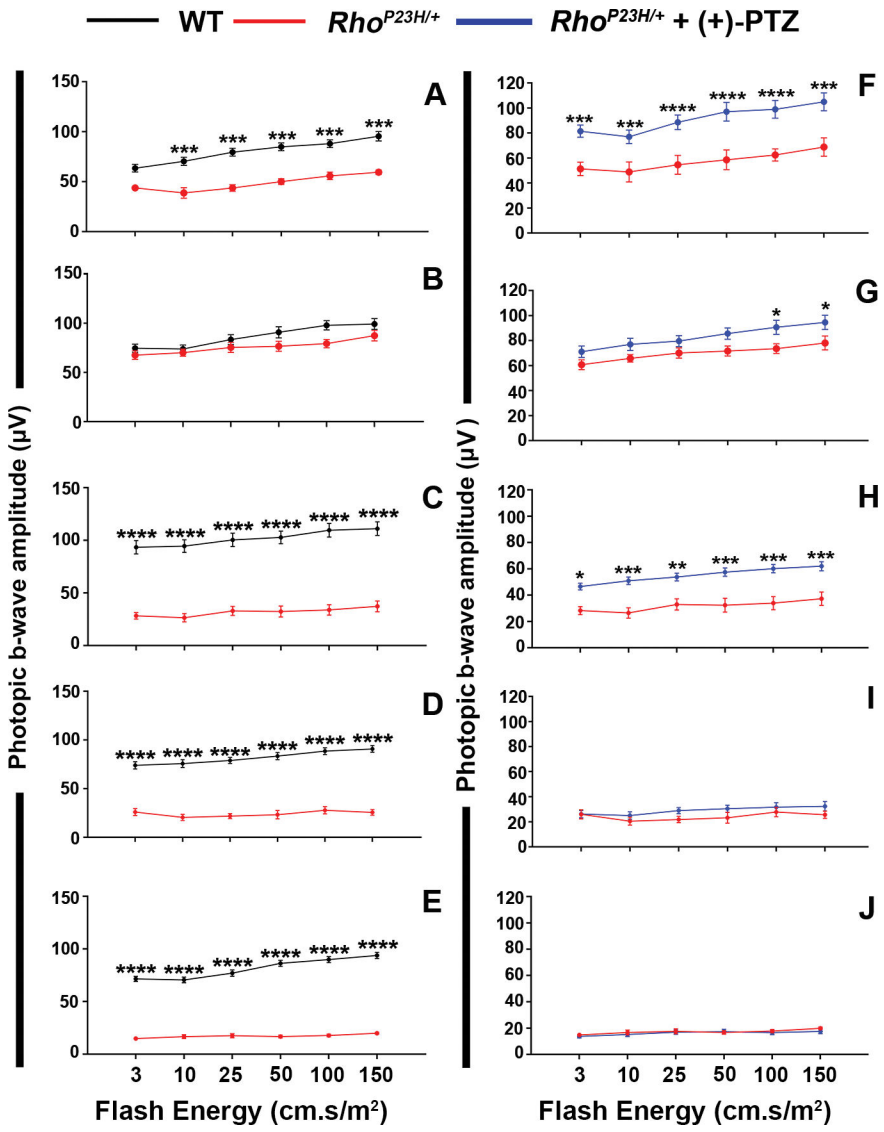

Figure 5: Analysis of photopic responses in female wild type, *Rho*$^{P23H/+}$ and *Rho*$^{P23H/+}$ + (+)-PTZ mice.

Light adapted (photopic) assessment of retinal function in female wild type and *Rho*$^{P23H/+}$ mice and *Rho*$^{P23H/+}$ + (+)-PTZ. Quantitative data from b-wave amplitudes for (A) 2 month (B) 4 month (C) 6 month (D) 8 month (E) 10 month female mice for wild type and *Rho*$^{P23H/+}$ plotted at the six light intensities described in the text. Quantitative data from b-wave amplitudes for (F) 2 month (G) 4 month (H) 6 month (I) 8 month (J) 10 month female mice for *Rho*$^{P23H/+}$ and *Rho*$^{P23H/+}$ + (+)-PTZ plotted at the six light intensities described in the text. Data were considered significant if the P-value was less than 0.05 (*0.05, **0.01, ***0.001, ****0.0001).

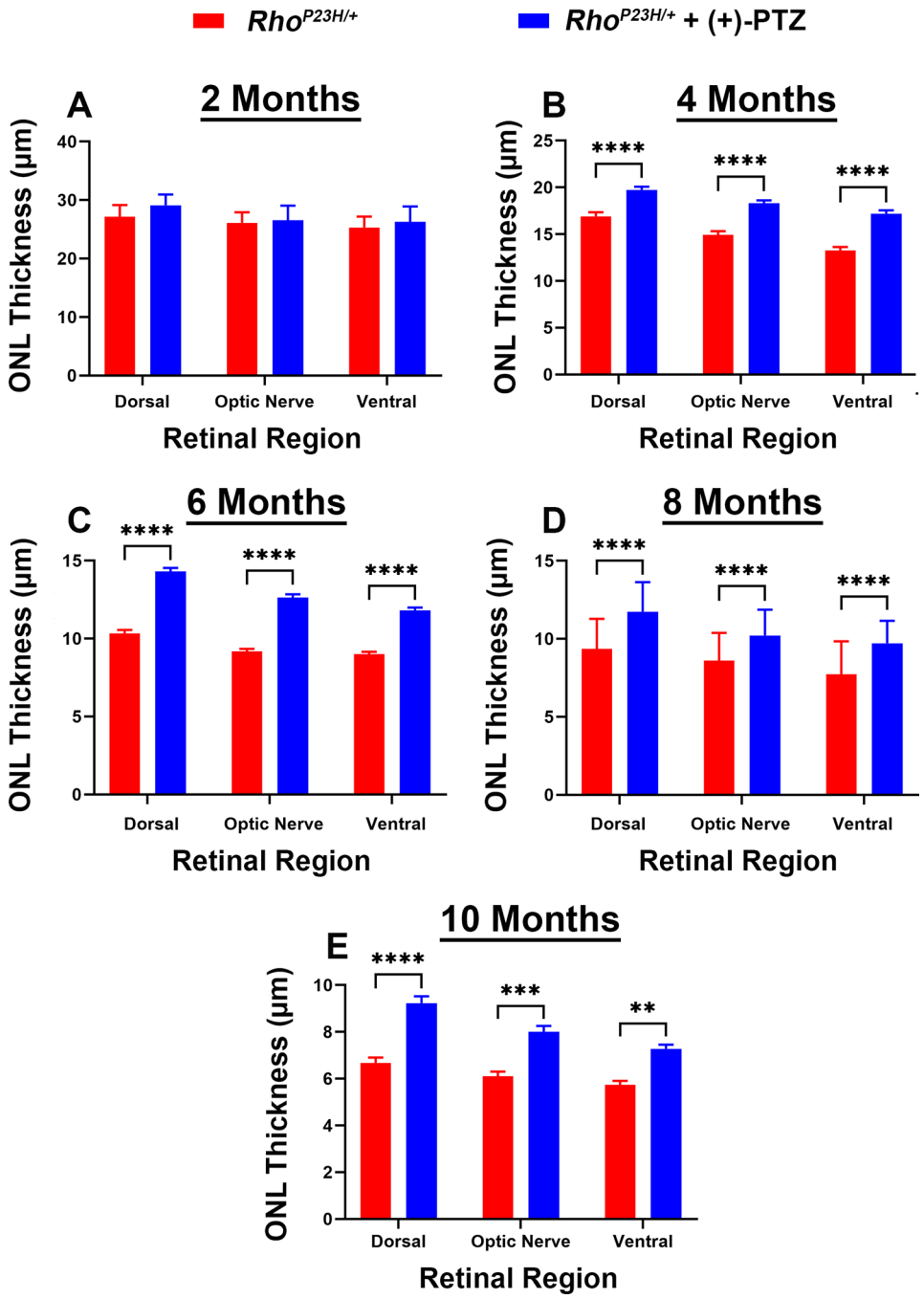

Figure 6: SD-OCT analysis of retinal ONL thickness in male *Rho*$^{P23H/+}$ and *Rho*$^{P23H/+}$ + (+)-PTZ mice.

Male *Rho*$^{P23H/+}$ and *Rho*$^{P23H/+}$ (+)-PTZ-treated mice were subjected to SD-OCT as described in the text. SD-OCT B-scans were obtained and ONL thickness quantified. Quantification of the ONL thickness from *Rho*$^{P23H/+}$ and *Rho*$^{P23H/+}$ (+)-PTZ-treated mice at (A) 2 month (B) 4 month (C) 6 month (D) 8 month and (E) 10 month. Data were considered significant if the P-value was less than 0.05 (*0.05, **0.01, ***0.001, ****0.0001).

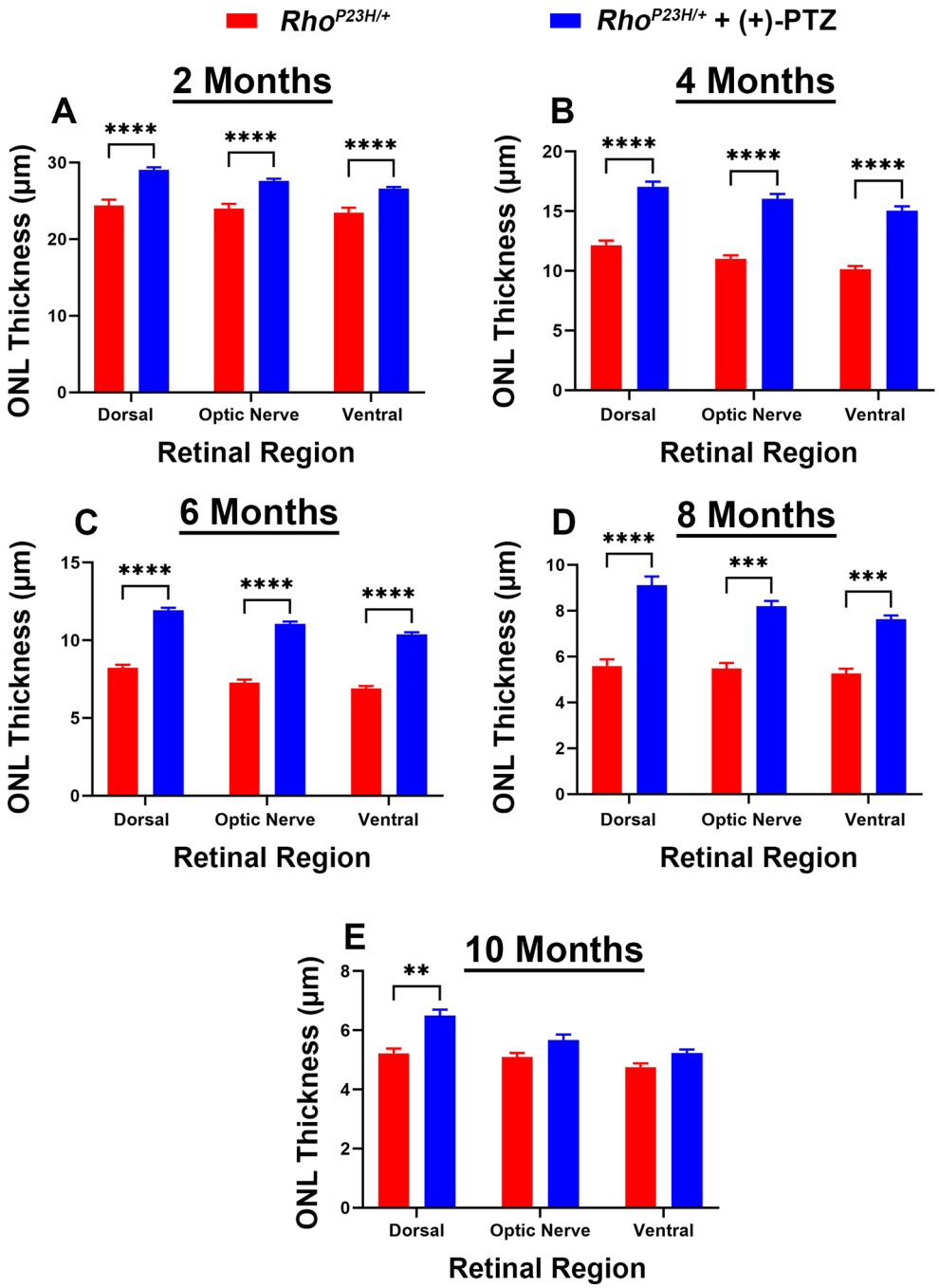

Figure 7: SD-OCT analysis of retinal ONL thickness in female *Rho*$^{P23H/+}$ and *Rho*$^{P23H/+}$ + (+)-PTZ mice.

Female *Rho*$^{P23H/+}$ and *Rho*$^{P23H/+}$ (+)-PTZ-treated mice were subjected to SD-OCT as described in the text. SD-OCT B-scans were obtained and ONL thickness quantified. Quantification of the ONL thickness from *Rho*$^{P23H/+}$ and *Rho*$^{P23H/+}$ (+)-PTZ-treated mice at (A) 2 month (B) 4 month (C) 6 month (D) 8 month and (E) 10 month. Data were considered significant if the P-value was less than 0.05 (*0.05, **0.01, ***0.001, ****0.0001).

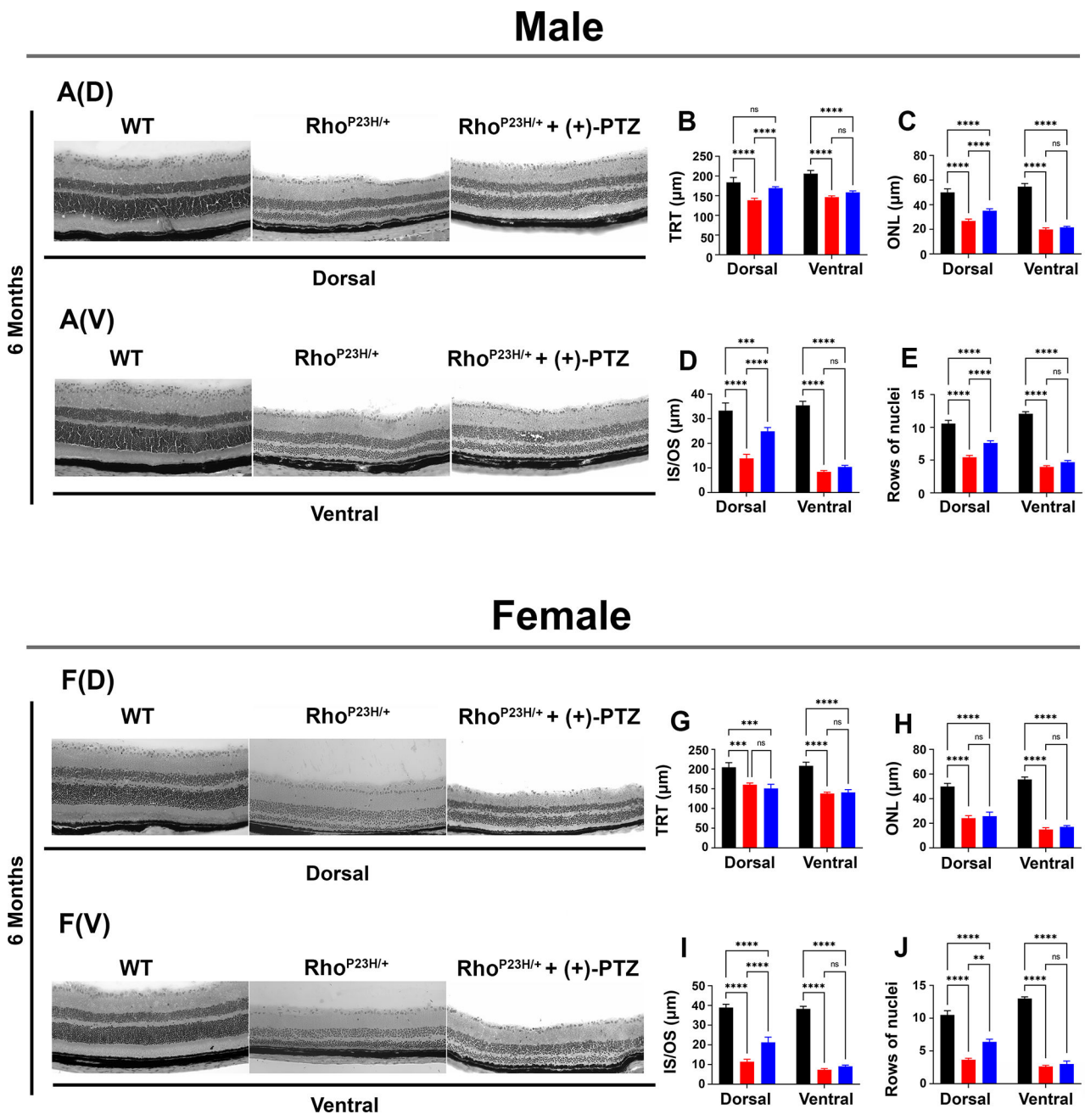

Figure 8: Morphometric analysis of male and female wild type, *Rho*$^{P23H/+}$, and *Rho*$^{P23H/+}$ + (+)-PTZ mice

Morphometric analysis was performed on male and female wild type, *Rho*$^{P23H/+}$, and *Rho*$^{P23H/+}$ + (+)-PTZ H&E stained retinal cryosections. (A) Representative images in male mice for both the (D) dorsal and (V) ventral retinas. (B-E) Quantification of the TRT, ONL, IS/OS thickness, and rows of nuclei in both the dorsal and ventral retina presented at 6 months in male mice. (F) Representative images in female mice for both the (D) dorsal and (V) ventral retinas. (G-J) Quantification of the TRT, ONL, IS/OS thickness, and rows of nuclei in both the dorsal and ventral retina presented at 6 months in female mice. TRT: Total retinal thickness, ONL: Outer nuclear layer, IS/OS: Inner and outer segment. Data

were considered significant if the P-value was less than 0.05 (*0.05, **0.01, ***0.001, ****0.0001).

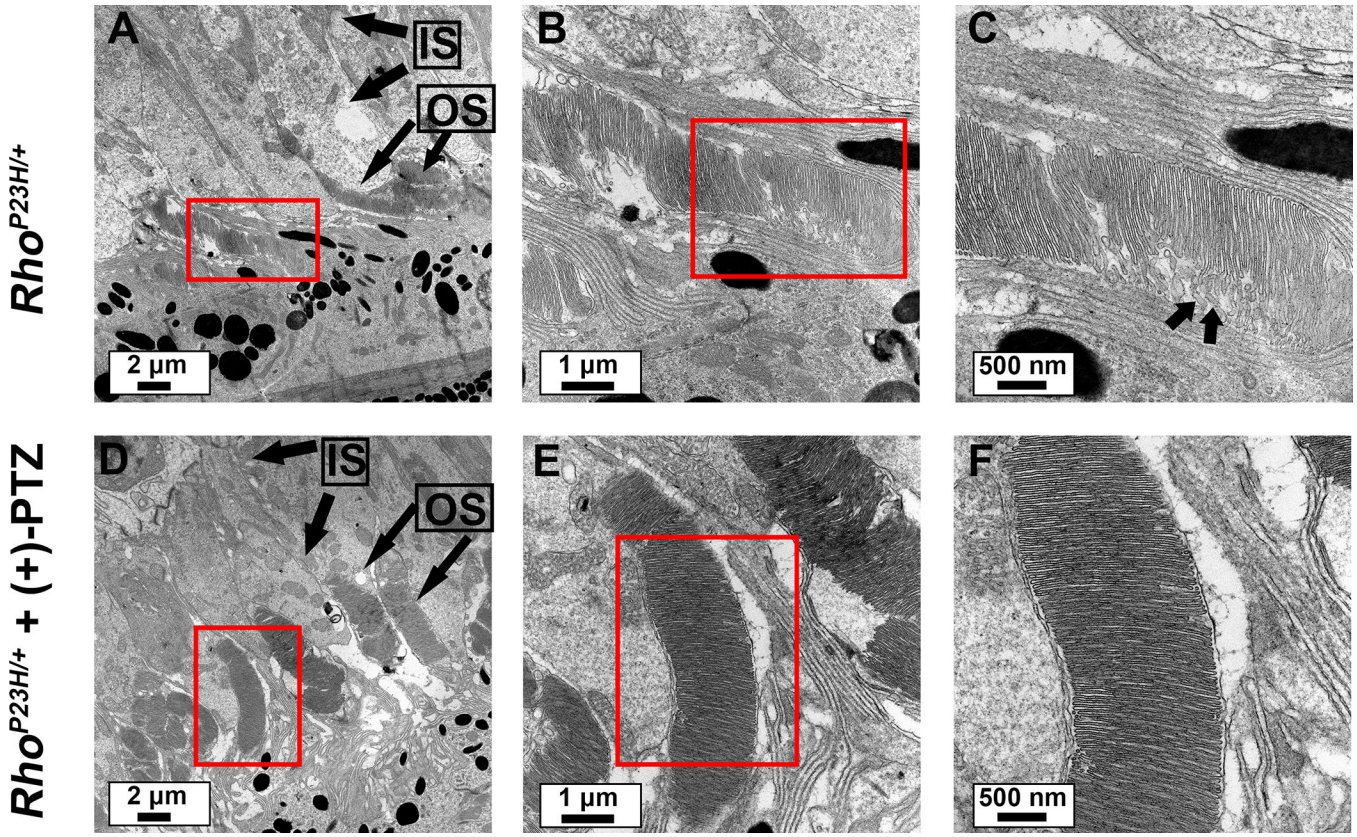

Figure 9: Transmission electron microscopy of male *Rho*$^{P23H/+}$ and *Rho*$^{P23H/+}$ + (+)-PTZ

Transmission electron microscopy was performed in 4 month old male *Rho*$^{P23H/+}$, and *Rho*$^{P23H/+}$ + (+)-PTZ retinas. Representative images of regions including the IS, OS, and RPE are shown. Insets show area of magnification that is visualized in the adjacent panel. Arrows: vesicles.

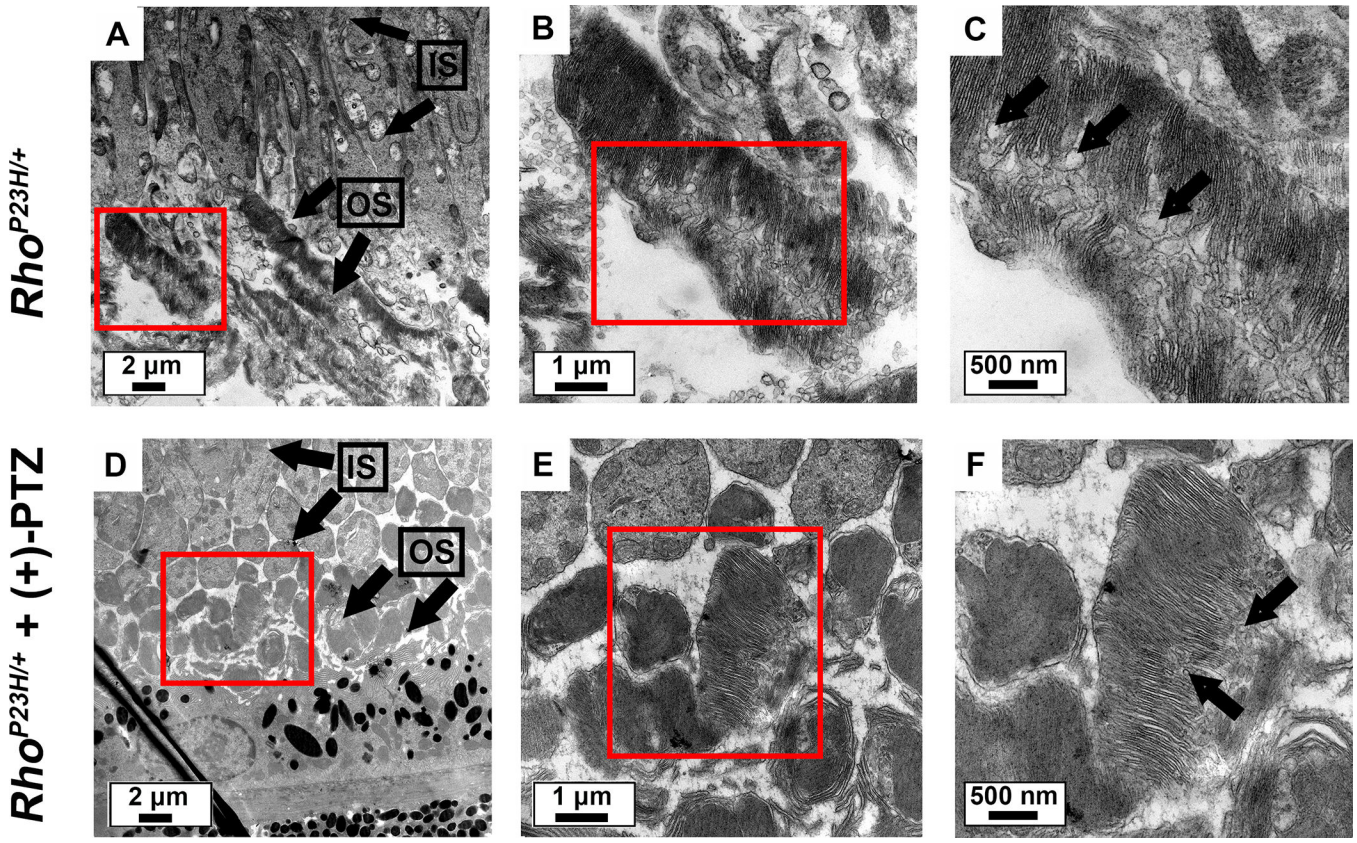

Figure 10: Transmission electron microscopy of female *Rho*$^{P23H/+}$ and *Rho*$^{P23H/+}$ + (+)-PTZ retinas.

Transmission electron microscopy was performed in 4 month old female *Rho*$^{P23H/+}$, and *Rho*$^{P23H/+}$ + (+)-PTZ retinas. Representative images of regions including the IS, OS, and RPE are shown. Insets show area of magnification that is visualized in the adjacent panel. Arrows: vesicles.